Applied Catalysis B: Environmental 201 (2017) 600–606

Contents lists available at ScienceDirect

Applied Catalysis B: Environmental

journal homepage: www.elsevier.com/locate/apcatb

Photoelectrocatalytic degradation of phenol-containing wastewater by TiO_2/g-C_3N_4 hybrid heterostructure thin film

Zhen Wei[a], Fenfen Liang[a], Yanfang Liu[b], Wenjiao Luo[a], Jun Wang[a], Wenqing Yao[a], Yongfa Zhu[a,*]

[a] Department of Chemistry, Tsinghua University, Beijing, 100084, China
[b] China Sinopec Research Institute of Petroleum Processing, Beijing, 100083, China

ARTICLE INFO

Article history:
Received 7 July 2016
Received in revised form 25 August 2016
Accepted 1 September 2016
Available online 1 September 2016

Keywords:
Photoelectrocatalytic
Synergistic effect
Surface hybrid heterojunction
Coking wastewater
Degradation phenolic compounds

ABSTRACT

TiO_2/g-C_3N_4 (TCN) thin film electrode was fabricated via a surface hybridization and dip-coating method. Phenol could be completely mineralized and the pollutants in coking wastewater could be degraded quickly by TCN under simulated solar light and electric field. The characteristics of the photoelectrocatalytic (PEC) degradation of phenol-containing coking wastewater were investigated under visible light, ultraviolet light and simulated solar irradiation. The results showed that phenol was degraded completely by the TCN-0.3 with a 1.5 V bias in 1.5 h under simulated solar irradiation with 100% TOC removal rate. 45% of the TOC for the coking wastewater was removed by the TCN-0.3 with a 1.5 V bias under 5.0 h simulated solar irradiation, which was 2.45 and 5.69 times as high as that of the pure TiO_2 and g-C_3N_4, respectively. The surface hybrid heterojunction formed between TiO_2 and g-C_3N_4 promotes the migration of the photogenerated electrons and holes and greatly improves the degradation efficiency with applied potential. The significant synergistic effect between the electrocatalytic and photocatalytic oxidation processes in PEC is conducive to electron-hole pair separation, producing the more active substances, such as hydroxyl radicals, and increases the degree of degradation and mineralization of phenolic compounds.

1. Introduction

Coking wastewater is generated from coal coking, coal gas purification, and by-product recovery processes of coking. It contains volatile phenol, polycyclic aromatic hydrocarbons and oxygen, sulfur, nitrogen and other heterocyclic compounds [1]. These compounds are teratogenic, mutagenic and carcinogenic, resulting in the serious toxicity of coking wastewater, which causes serious pollution problems to the whole world [2]. More seriously, phenolic compounds are persistent organic contaminants, exhibiting low biodegradability and thus posing serious and long-term risks to human health once discharged into natural water. Phenol was more difficult to degrade compared to those chlorinated and nitro-substituted phenolic compounds, both of which need to deal with the depth of discharge [3].

A number of physical, chemical and biological methods have been applied to remove or degrade phenolic compounds in coking wastewater [4]. The conventional treatment process of coking wastewater is the activated sludge process. It consists of solvent extraction of phenolic compounds and steam stripping of ammonia, followed by biological treatment [5]. Since a certain number of refractory and inhibitory organic compounds in coking wastewater are highly concentrated, the conventional activated sludge process is not effective for COD removal [6].

Advanced oxidation processes (AOPs) have been the rise of new technologies in the field of water treatment in the last 20 years [7], which are widely applied to the treatment of bio-refractory organic contaminants in the industrial wastewater [8,9]. Photocatalysis (PC) is one of the most efficient AOPs. It can produce highly reactive hydroxyl radicals (•OH) to oxidize organic pollutants at ambient temperature and pressure. TiO_2 is widely recognized as the great potential and powerful photocatalyst for its chemical stability, low-cost, eco-friendly and high reactivity [10]. Nevertheless, the TiO_2 utilization efficiency of solar energy was still very low due to the rapid recombination of photogenerated electron–hole pairs and poor response to visible light [11].

Photoelectrocatalytic (PEC) technology was one of the most popular and effective strategies to inhibit recombination of the electron–hole pairs photogenerated in heterogeneous semiconductor photocatalysis [12–14]. Compared to the pure PC

* Corresponding author.
E-mail address: zhuyf@tsinghua.edu.cn (Y. Zhu).

http://dx.doi.org/10.1016/j.apcatb.2016.09.003
0926-3373/

degradation system, the catalyst was immobilized on the conducting substrate to serve as the photoanode in the PEC system. It could be easily separated and recycled after the catalytic reaction [15]. In the PEC process, a potential bias is applied to the photoanode, which provides an external driving force that can promote the photogenerated electrons to move faster through the external circuit to the cathode. Thus, the recombination rate of photogenerated electrons and holes is minimized [16–18]. More importantly, combining the advantages of the heterogeneous PC and electrocatalytic (EC) process, the PEC process is more efficient in degrading organic pollutants and inactivating bacteria compared with both pure PC and EC processes.

To overcome the poor visible light response, numerous approaches have been investigated to improve the visible-light utilization of TiO_2, such as doping, dye sensitization, heterojunction and hybridization construction and so on [19–25]. Graphitic carbon nitride (g-C_3N_4), as a metal-free conjugated semiconductor photocatalytic material, was first reported for hydrogen evolution under visible light ($\lambda > 420$ nm) in 2009 [26,27]. More and more attention has been paid to g-C_3N_4 because of its high physicochemical stability, outstanding electronic band structure and environmentally benign characteristics [28–30]. g-C_3N_4 can be combined with many ultraviolet light responsive photocatalysts to enhance their activity under visible light, such as $BiPO_4$ [31], ZnO [32], and TiO_2 [33]. In spite of these appealing properties, g-C_3N_4 is difficult to completely mineralize phenolic compounds by itself [34,35], limiting its application in the field of environment treatment.

This work composited TiO_2 with g-C_3N_4 nanosheets to prepare new and efficient TiO_2/g-C_3N_4 (TCN) surface hybrid heterojunction structure composites. The morphology, structure, optical and photoelectric properties of TCN were investigated systematically. The effects of g-C_3N_4 content, the light source and bias voltage on the PEC degradation of phenol and coking wastewater, as well as the TOC removal rate were investigated in detail. The mechanism of the degradation process and the synergetic effect between photocatalysis and electrocatalytic processes were discussed.

2. Experimental

All chemicals were analytical-grade reagents and purchased from Aladdin Chemical Reagent Co., Ltd. and used as received without further purification in the experiments. Indium-tin oxide (ITO) glass (a sheet resistance: 15 Ω/square; size: 20 mm × 40 mm; thickness: 1.1 mm) was purchased from China Southern Glass Co. Ltd.

2.1. Chemical exfoliation of g-C_3N_4

The metal-free g-C_3N_4 was synthesised by thermally decomposing melamine at 823 K with a ramp rate of 2 K min^{-1} in an alumina crucible. Then kept it at 823 K for 4 h in static air and cooled to room temperature naturally. The yellow product was obtained and ground to fine powder for further use.

Chemical exfoliation method was used to prepare g-C_3N_4 nanosheets [34]. The as-synthesised g-C_3N_4 (2 g) was dissolved in 50 mL 98% concentrated sulfuric acid and stirred vigorously for 8 h (the reaction temperature kept at 298 K). Then, the reaction solution was tardily diluted in 500 mL water and sonicated for exfoliation. In this process, large amount of heat was released and the color of the suspension turned to light yellow. Afterwards, the suspension was centrifuged at 2000 rpm for 10 min to remove the unexfoliated g-C_3N_4. The procured light yellow product was further centrifuged, washed repeatedly with deionized water to near neutral pH, and dried at 353 K for 24 h. The obtained products were g-C_3N_4 nanosheets.

2.2. Synthesis of TiO_2/g-C_3N_4 surface hybrid compounds

0.5 g of the exfoliated g-C_3N_4 was added into 100 mL of deionized water and then ultrasonically treated for 6 h to form the more stable g-C_3N_4 dispersion. A certain amount of TiO_2 powder (Degussa P25) was added into the dispersion, ultrasonically dispersed for 2 h and stirred for 0.5 h. Then the dispersion was centrifuged and the resulting powder was dried in an oven at 353 K. By grinding the resulting sample, TiO_2/g-C_3N_4 composite photocatalyst was obtained. They were marked as TCN-X, X labelled as g-C_3N_4 mass ratio in the composite. They were 0.05, 0.1, 0.2, 0.3, and 0.4, respectively.

2.3. Fabrication of the TiO_2/g-C_3N_4 film electrodes

The TiO_2/g-C_3N_4 film electrodes were fabricated via a dip-coating method on ITO glass [36]. 200 mg of the TiO_2/g-C_3N_4 powder was dispersed in 250 mL water by ultrasonication for 6 h at room temperature. After that, the ITO glass was immersed in the TiO_2/g-C_3N_4 suspension and a typical dip-coating procedure parameters were as follows: the lifting height was 3.5 cm, the dipping time was 60 s and the dipping-pulling rate was 50 μm/s. The dip-coating steps were repeated for three times and the film electrodes were dried for 1 h at 353 K after each dip-coating process. The thickness of TCN-0.3 films reached to 1, 1.5 and 2.5 μm when it was dip-coated one, three and five times, respectively (Fig. S4). When dip-coated three times, the PEC degradation activity enhancement most (Fig. S5), so the optimal dip-coating steps was three times.

2.4. Characterization

The morphologies of TCN were examined by electron microscope operated on Hitachi HT 7700 at an accelerating voltage of 100 kV and high-resolution transmission electron microscope (HRTEM) on JEOL JEM-2100F field emission transmission electron microscope operated at an accelerating voltage of 200 kV. FESEM images were characterized on a Hitachi SU-8010 Field Emission Gun Scanning Electron Microscopy. TCN samples were characterized by X-ray diffraction (Rigaku D/max-2400 X-ray diffractometer) with Cu Kα1 ($\lambda = 0.15418$ nm) radiation at 40 kV and 200 mA to investigate the phase structure. UV–visible diffuse reflectance spectra (DRS) of TCN were obtained by using Hitachi U-3010 spectrophotometer using barium sulfate as a reference. The room-temperature photoluminescence (PL) spectra of TCN were recorded on Perkin-Elmer LS55 spectrophotometer with an excitation wavelength of 370 nm.

2.5. Degradation activity and PEC measurements

The EC and PEC measurements were recorded on CHI 660 B (Chenhua, China) electrochemical system workstation. The measurements were conducted in 0.1 M Na_2SO_4 electrolyte solution with a three-electrode cell system. Platinum wire (70 mm in length and 0.4 mm in diameter) was used as the counter electrode and saturated calomel electrode (SCE) was used as a reference electrode. Xenon lamp (500 W) or mercury lamp (15 W, 90% of the energy output at 254 nm) was placed at a distance of 15 cm in front of the film electrodes. The visible irradiation was obtained by the Xenon lamp with 420 nm cutoff filter and the average light intensity was 35 mW/cm^2. The ultraviolet light intensity was 0.69 mW/cm^2.

PEC and EC degradation experiments were carried out in a cuboid (5 × 5 × 10 cm) quartz glass reactor. The degraded pollutants were 100 mL phenol with the initial concentration of 5 mg/L or coking wastewater with the initial TOC of 25 ppm. Sodium sulfate was used as electrolyte solution with the concentration of 0.1 M. The film electrodes were submerged 2.5 cm in solutions

vertically. 3 mL solutions were sampled every 30 min and the particles were separated by high-speed centrifugation and filtrated with a 0.45 μm Millipore filter. The concentration of phenol was detected by the HPLC (Agela Technologies Inc.) analysis with an UV absorbance detector (K 2501) at 270 nm and Venusil XBP-C_{18} using as a reversed phase column. The mobile phase was CH_3OH and H_2O (60:40, v/v) with a flow rate of 1 mL/min. The total organic carbon (TOC) was applied to analyse the mineralization degree of organic contaminants on Analytik Jena AG (Multi N/C 2100).

3. Results and discussion

3.1. Morphology structure and optical properties

Fig. 1A and C are the typical TEM and SEM images of TiO_2/g-C_3N_4 composites(30 wt.% g-C_3N_4). It can be seen the exfoliated g-C_3N_4 samples were very transparent nanosheets, indicating their ultrathin thickness [34]. The HRTEM image of TiO_2/g-C_3N_4 (Fig. 1B) shows the clear lattice fringes of TiO_2 (d = 0.35 nm corresponding of TiO2 (101)), as well as the intimate vague fringes of g-C_3N_4. This intimate contact enables the formation of surface hybrid heterojunction structure between TiO_2 and g-C_3N_4, which is conducive to charge separation [37]. Based on the XRD results, the main diffraction peak of the TiO_2/g-C_3N_4 composite was at θ = 25.2°, which is the characteristic peak of the anatase phase. The intensity of this peak did not change significantly with the increase of g-C_3N_4 content. The (002) plane of the stacking of the conjugated aromatic system in g-C_3N_4 and the diffraction peak of rutile phase (110) plane overlapped at θ = 27.4°. As the content of g-C_3N_4 increased, this overlapped peak became wider and stronger.

Fig. 2A shows the UV–vis diffuse reflectance spectra of TiO_2, g-C_3N_4 and TiO_2/g-C_3N_4 (TCN). It can be seen that the absorption edge of TiO_2 and g-C_3N_4 are 380 nm and 460 nm, respectively. Based on the calculation results, the band gap of TiO_2 and g-C_3N_4 were 3.26 eV and 2.70 eV, respectively. The band edges of TCN composites were all between that of TiO_2 and g-C_3N_4. Compared with pure TiO_2, the absorption edge of TCN photocatalysts had a red shift with increasing amounts of g-C_3N_4. The band gap of TCN-0.3 was 2.95 eV, expanding to the visible light region. This is attributed to the presence of g-C_3N_4 on TiO_2 surface. Therefore, surface hybrid heterostructure of TiO_2 and g-C_3N_4 was formed in TCN composites [38,39].

The recombination rate of free charge carriers can be measured by photoluminescence (PL) spectra [40–42]. Compared with the fluorescence emission spectra (Fig. 2B) of g-C_3N_4, the emission peak of TCN-0.3 shown an obvious blue-shift and its intensity decreased significantly. This indicates that electrons can transit from the more negative conduction band of g-C_3N_4 to the conduction band of TiO_2 ($E_{CB,g\text{-}C3N4} = -1.12$ eV, $E_{CB,TiO2} = -0.5$ eV), indicating the formation of hybrid heterojunction structure between g-C_3N_4 and TiO_2 could promote the transfer of photogenerated electrons and holes and thus the recombination of electrons and holes is suppressed [41,43].

3.2. Photoelectric properties

A bias voltage is applied between the photocatalyst film electrode and the Pt electrode, forming an electric field. Due to this electric field, the photogenerated electrons and holes move in the opposite direction, resulting in their accelerated separation rate, and meanwhile, their recombination possibility reduced. This phenomenon can be detected directly by the change of photocurrent [44,45]. TiO_2 did not respond to visible light, and its photocurrent was zero. However, the composite responded to visible light obviously. In addition, as the content of g-C_3N_4 increased, the photocurrent increased (Fig. 2C). When it increased to 30%, the photocurrent reached the maximum value (Ip = 3.6 μA). Further increasing the content led to the decrease of photocurrent. This may result from the excessive g-C_3N_4, which agglomeration could hinder the migration and separation of photo-generated electrons and holes.

Fig. 2D is a comparison of the linear scan intermittent current among g-C_3N_4, TiO_2 and TCN-0.3. As can be seen, even if the bias voltage is increased, the photocurrent of TiO_2 shows no significant change under visible light. By comparison, the photocurrent of g-C_3N_4 and TCN-0.3 film increased as the bias voltage increased. The bias of the range TCN-0.3 composite wider photocurrent is also larger, indicating that the hybrid heterojunction structure is also conducive to the separation of photo-generated charge, can effectively reduce the photo-generated carriers compound, thereby help to improve its photocatalytic activity [46].

3.3. Effect of g-C_3N_4 content on the catalytic activity of TiO_2/g-C_3N_4 photocatalytic

Due to the high recombination rate of photo-generated electrons and holes, the visible light photocatalytic activity of g-C_3N_4 is not high. As can be seen from Fig. 3A, only 8.9% of phenol was removed by g-C_3N_4 after 5 h visible light irradiation. TiO_2 has no photocatalytic activity under visible light. As for g-C_3N_4 and TiO_2 hybrid composite, the degradation efficiency of phenol increased as the content of g-C_3N_4 increased. When the content of g-C_3N_4 increased to 30% (TCN-0.3), the degradation efficiency of phenol reached the maximum of 22.3% under visible light, which is 2.5 times as high as that of the pure g-C_3N_4. Under ultraviolet light, the results are similar. When g-C_3N_4 accounted for 30%, the degradation efficiency of phenol reached the maximum value of 47.6%, which is four times as high as that of the pure g-C_3N_4 and 2.8 times of TiO_2. Further increasing the amount of g-C_3N_4, the photocatalytic degradation activity of the composite decreased and the degradation efficiency of TCN-0.4 was 14.5% under visible light and 41.8% under UV light. When the content of g-C_3N_4 was lower, the number of photogenerated electrons was limited and they are much easier to recombine with a hole. The chemical exfoliation of g-C_3N_4 nanosheets are prone to agglomeration when the g-C_3N_4 content was high, resulting in the reduced reaction active sites and lower photocatalytic activity [47]. Therefore, the optimal ratio of g-C_3N_4 was 30%. At this point, agglomeration of g-C_3N_4 nanosheets is slight and the surface hybrid heterojunction structure forms, which largely contributes to the separation of electron-hole pairs.

3.4. Effect of bias potential on photoelectrocatalytic activity of TiO_2/g-C_3N_4

TCN-0.3 was selected as a typical sample for studying the EC and PEC degradation of phenol. Fig. 3B shows the EC degradation efficiency of phenol at different bias potentials in 5 h. The degradation efficiency of phenol gradually increased as the bias potential increased in the range of 0.5–2.5 V. When the bias voltage was 2.5 V, the EC degradation efficiency of phenol reached the maximum of 90.2%. However, the phenol degradation efficiency decreased when the bias voltage further increased. It dropped to 17.9% at 3.5 V bias voltage, which may be due to the formation of phenol-based polymers hindering the further degradation of phenol [36,48].

As can be seen from Fig. 3B, the EC degradation efficiency of phenol was greatly increased by the visible light. In addition, the PEC degradation efficiency of phenol increased as the bias potential increased in the range of 0.5–1.5 V, and complete degradation of phenol was achieved when the potential was 1.5 V or higher. The increased degradation efficiency of phenol by the increasing bias voltage can be explained as follows: The bias voltage can increase the width of the space charge layer, which can promote

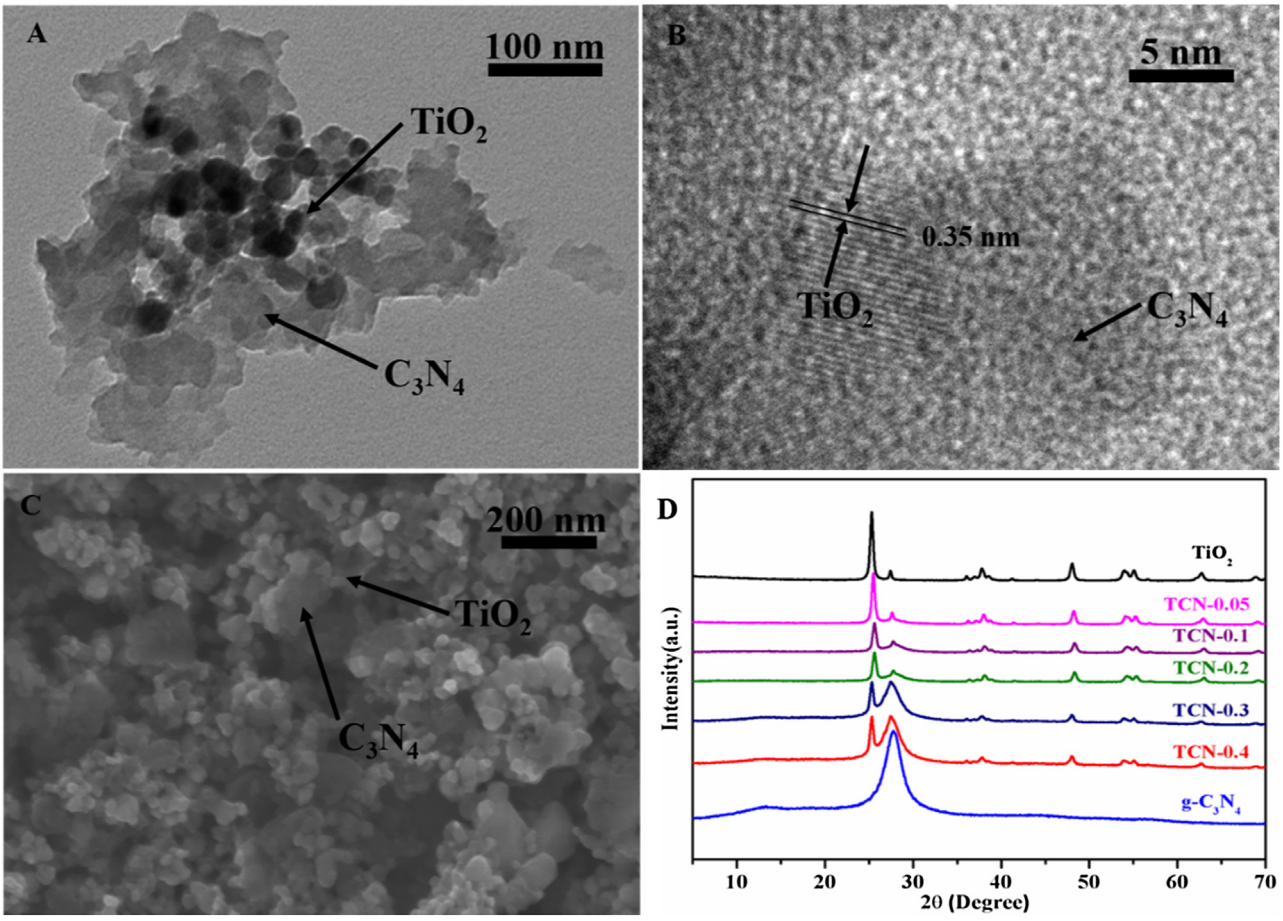

Fig. 1. TEM (A), HRTEM (B) and SEM (C) images of TCN-0.3; XRD patterns (D) of g-C_3N_4, TiO_2 and TCN photocatalysts.

the separation and refrain the recombination of photogenerated carriers. As the voltage increased, the increment of the space charge layer's width increased, and hence the PEC degradation efficiency of phenol increased. However, when the bias voltage was higher than 2.5 V, the width of the space charge layer cannot be further increased, since the electrons generated from the photocatalytic process is constant under fixed light intensity. Therefore, the degradation rate of phenol did not increase when the bias potential was higher than 1.5 V. When the bias voltage higher than 2.5 V, the degradation rate of phenol decreased due to the reallocation of the space charge layer and the Hector Helmholtz layer. This reallocation would result in the reduced the number of photogenerated carriers and thus the decreased degradation rate of phenol. At 3.5 V bias conditions, the degradation efficiency of phenol decreased to 52.8%. Based on the above results, the optimum voltage in this experiment is 1.5 V and this voltage is adopted in the following experiments.

3.5. Photoelectrocatalytic mineralization of phenol and coking wastewater

To study the photoelectrocatalytic degradation efficiency of phenol by TiO_2/g-C_3N_4 samples, different light sources were utilized at a bias voltage of 1.5 V. As can be seen from Fig. S1, S2 and S3, phenol could be completely degraded bmation of hybrid heterojunction in 2 h visible light irradiation, 1 h UV irradiation and 1.5 h simulated solar irradiation. g-C_3N_4 or TiO_2 alone requires 3 h or more time to achieve complete degradation of phenol under different light sources with 1.5 V bias potential. As can be seen from the rate constant values of g-C_3N_4, TiO_2 and TiO_2/g-C_3N_4 (Fig. 4A), TiO_2/g-C_3N_4 was more efficient than pure g-C_3N_4, and TiO_2 under UV, visible and simulated solar light. Furthermore, to do a simple addition, we can see that the rate constant of TiO_2/g-C_3N_4 was larger than the sum of that of pure g-C_3N_4 and TiO_2. This indicates that the surface hybrid heterostructure formed between TiO_2 and g-C_3N_4 can significantly enhance the activity of TiO_2/g-C_3N_4 composite. The PEC activity of TCN-0.3 under UV irradiation is almost 2.6 times as high as that of TiO_2 and 2.2 times of g-C_3N_4 under visible light. When used Xe lamp to simulate solar irradiation, The PEC activity of TCN-0.3 is 2.88 times of g-C_3N_4 and 2.4 times of TiO_2.

As stated earlier, the ability to deep mineralize organic pollutants is crucial for environmental governance. During many EC, PC or PEC processes, phenol was conversed to more poisonous benzoquinone and hydroquinone rather than mineralized to CO_2 and H_2O. In this work, TOC was employed to evaluate the mineralization efficiency of phenol under different experimental conditions. As can be seen from Fig. 4B, only 32.6% and 54.3% TOC was removed by pure g-C_3N_4 and TiO_2 with 1.5 V bias potential under simulated solar irradiation in 3 h. By comparison, 100% TOC removal rate could be achieved when TCN-0.3 composite were utilized, indicating the improved mineralization degree.

Coking wastewater is a very serious conundrum to the world since it contains strong toxic phenolic compounds, polycyclic aromatic hydrocarbons compounds and so on [2,49]. To evaluate the efficiency of TCN-0.3 in mineralizing coking wastewater, TOC removal rate was examined in the PEC degradation process of coking wastewater under simulated solar irradiation at a bias voltage of 1.5 V. Less than 10.0% of the TOC in coking wastewater was removed by Pure g-$C_3N_4$and 18.3% was removed by pure TiO_2. By comparison, 45.0% was removed by TiO_2/g-C_3N_4 composite (TCN-0.3) in 5 h (Fig. 4C). This result indicates that the surface hybrid hetero-

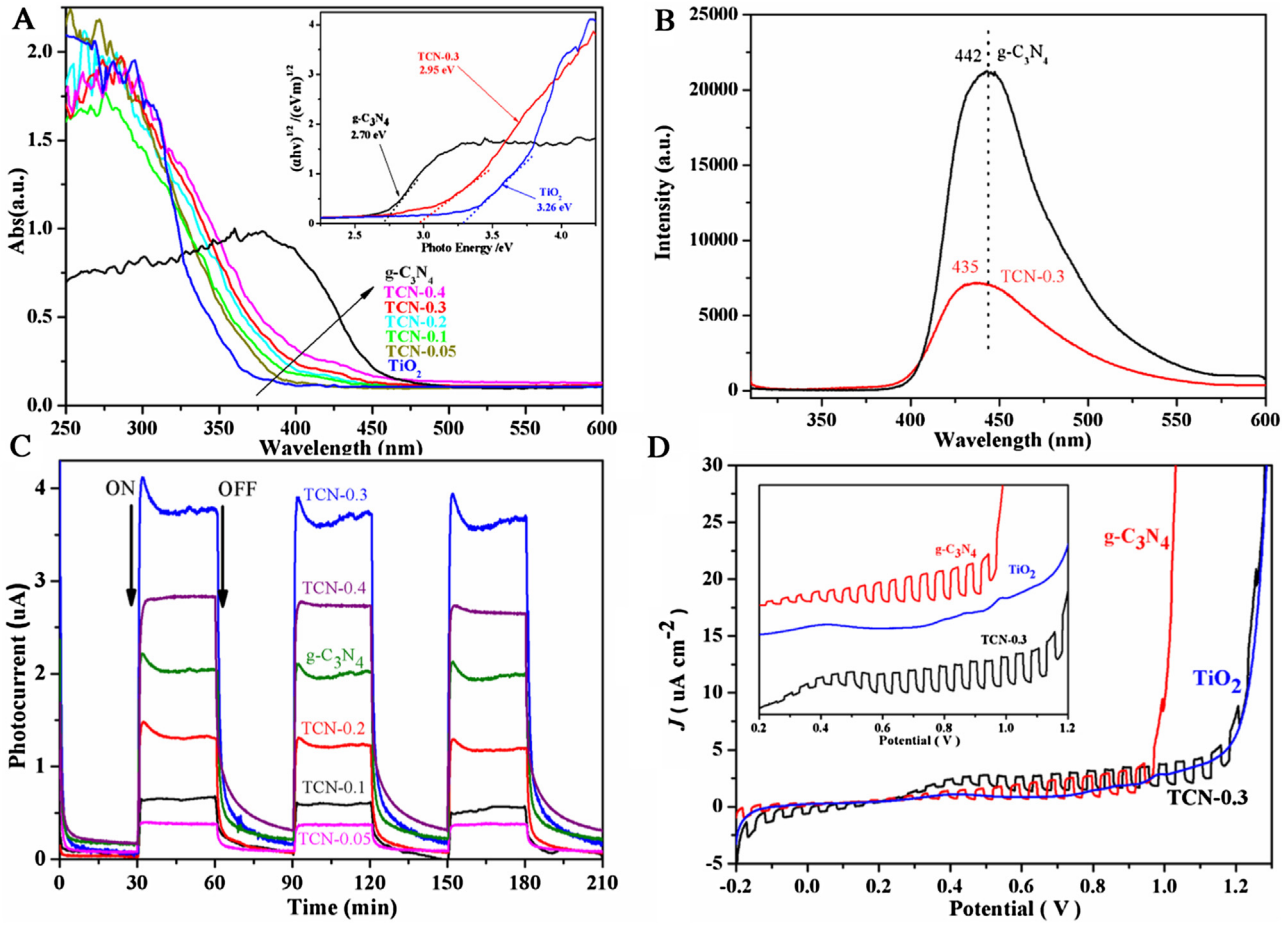

Fig. 2. (A) DRS spectra of g-C_3N_4, TiO_2 and TCN photocatalysts; (B) PL spectra of g-C_3N_4, and TCN-0.3 in different wavelength ranges; (C)Photocurrent measurements under visible light irradiation (λ > 420 nm) of g-C_3N_4 and TCN film electrodes in 0.1 M Na_2SO_4 aqueous solution. (D)Potentiodynamic scans under chopped illumination (λ> 420 nm) for g-C_3N_4, TiO_2 and TCN-0.3 film electrodes in 0.1 M Na_2SO_4 aqueous solution.

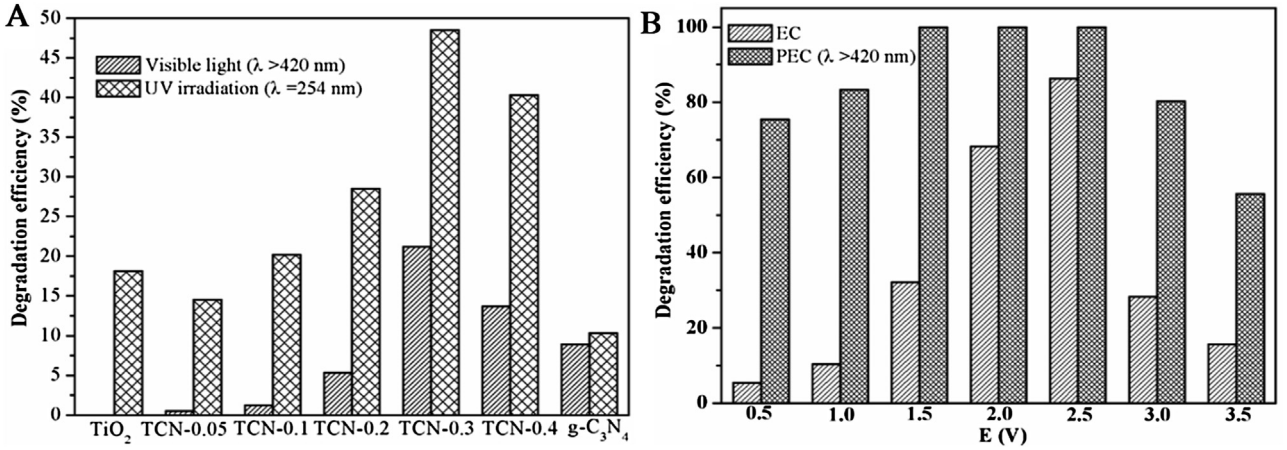

Fig. 3. (A) Photocatalytic degradation of phenol on various film electrodes in 0.1 M Na_2SO_4 solution under visible light (λ > 420 nm) or UV irradiation (λ= 254 nm); (B) Electrocatalytic and photoelectrocatalytic (visible light λ >420 nm) degradation of phenol on TCN-0.3 electrode at various potentials in 0.1 M Na_2SO_4 solution. (The concentration of phenol was 5 ppm.).

junction structure of the composite photocatalyst can enhance the mineralization efficiency of coking wastewater.

3.6. Synergistic catalytic degradation mechanism

The main active species of g-C_3N_4 is superoxide radical during the PC process [50], while holes are the main active species of the TiO_2 [10], so the main oxidation active species of TiO_2/g-C_3N_4 composite may be the hole and superoxide radicals. However, based on the active species trapping results, the main active species were different during the PEC process. The hydroxyl radicals, holes and superoxide radicals during the PEC degradation of phenol over TCN-0.3 were investigated with the addition of tertiary butanol (•OH scavenger)[51], EDTA-2Na (holes scavenger)[52],

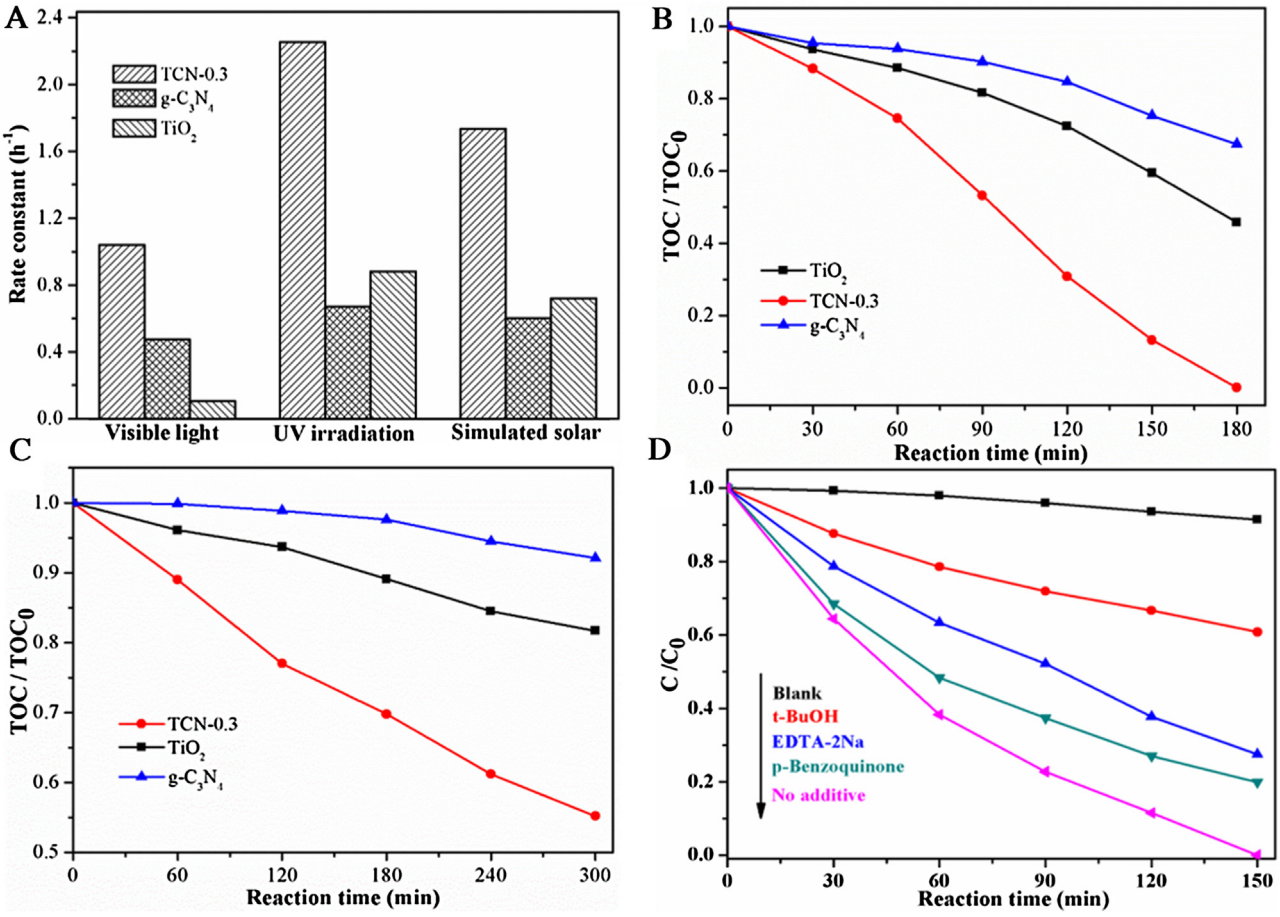

Fig. 4. (A)The rate constants for PEC degradation of phenol by g-C_3N_4, TiO_2 and TCN-0.3 film electrodes under different light irradiation conditions; (B) The change of TOC in the PEC degradation of phenol by g-C_3N_4, TiO_2 and TCN-0.3 electrodes under simulated solar irradiation (full spectrum) and 1.5 V bias potential; (C) The change of TOC in the PEC degradation process of coking wastewater by TCN-0.3 electrode under simulated solar irradiation (full spectrum) and 1.5 V bias potential. (D)The plots of photogenerated carriers trapping on PEC process by TCN-0.3 under visible light (λ > 420 nm) and 1.5 V bias potential.

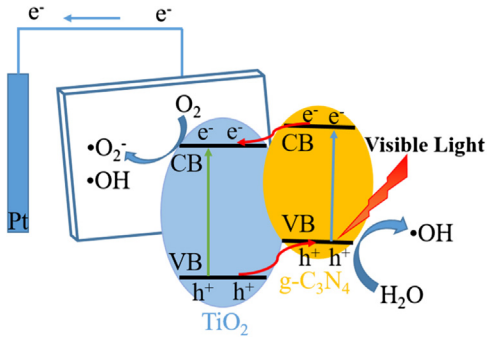

Fig. 5. PEC degradation mechanism by TCN-0.3 electrode.

p-benzoquinone ($^{\bullet}O_2^-$ scavenger)[53]. The addition of trapping agents could decrease the PEC degradation rate of phenol with different degree. Among them, tertiary butanol decreased the rate most significantly shown in Fig. 4D, indicating that the hydroxyl radicals are the major oxidative species in the mineralization of phenol by TiO_2/g-C_3N_4 composite.

Based on the band gap structure of g-C_3N_4 and TiO_2, the PEC degradation mechanism was proposed and illustrated in Fig. 5. As can be seen, the photogenerated electrons in g-C_3N_4 nanosheets can easily transfer to TiO_2 since the conduction band potential of the g-C_3N_4 is lower than TiO_2. On the other hand, the valence band potential of TiO_2 is higher than g-C_3N_4, and thus the photogenerated holes on the surface of TiO_2 can easily transfer to the valance band of g-C_3N_4. To realize the efficient transfer of photogenerated charge carriers, the formation of surface hybrid heterojunction structure is of great importance. It is crucial in suppressing the recombination of electrons and holes.

On the one hand, the light irradiation promoted the electrocatalytic oxidation. The anodic current density significantly increased with increasing the bias potential and oxygen could be generated when the applied potential was higher than 1.4 V [54,55]. As an electron acceptor, oxygen could accept electrons and combine with hydrogen ions, producing hydrogen peroxide on the TCN-0.3 electrode (Eq. (1)). However, the oxidation ability of H_2O_2 was not high enough to completely mineralize phenol. The hydroxyl radicals could be generated through Eq. (2) and (3), promoting the mineralization of phenols and other organic substances in wastewater.

$$O_2 + 2H^+ + 2e^- \rightarrow H_2O_2 \quad (1)$$

$$H_2O_2 + e^- \rightarrow {}^{\bullet}OH + OH^- \quad (2)$$

$$h^+ + OH^- \rightarrow {}^{\bullet}OH \quad (3)$$

On the other hand, the photocatalytic efficiency was improved by the bias potential. The photogenerated electrons transferred to the platinum electrode quickly through an external circuit with the assisted electric field. It promoted the photogenerated carriers to spatially separate and hence reduced the recombination rate of electron-hole pairs. The utilization of holes was improved due to generate hydroxyl radicals on the electrode surface (Eq. (3)) and

preventing the oxidation of the intermediate product restored in the cathode.

4. Conclusion

TiO_2/g-C_3N_4 thin film electrode was fabricated via a surface hybridization and dip-coating method. This composite film was efficient in photoelectric degradation of phenol and wastewater. Under simulated solar irradiation, the TCN-0.3 composite could completely mineralize phenol at a bias voltage of 1.5 V in 1.5 h. In addition, 45% of the TOC in coking wastewater was removed in 5 h solar irradiation which was 5.69 times higher than that of pure g-C_3N_4 (7.9%) and 2.45 times of TiO_2 (18.3%). The enhanced photocatalytic activity and mineralization efficiency of TiO_2/g-C_3N_4 composite are attributed to the formation of surface hybrid heterojunction structure between g-C_3N_4 and TiO_2. This heterojunction can effectively suppress the recombination rate of photogenerated electrons and holes, and thus improves the PEC efficiency. In addition, the synergistic effect between photocatalysis and electrocatalysis significantly improves the degradation and mineralization efficiency of phenolic compounds, making the PEC process an effective method to deal with coking wastewater.

Acknowledgments

This work was partly supported by National Basic Research Program of China (973 Program) (2013CB632403) and Chinese National Science Foundation (21437003, 21673126).

Appendix A. Supplementary data

Supplementary data associated with this article can be found, in the online version, at http://dx.doi.org/10.1016/j.apcatb.2016.09.003.

References

[1] S. Shi, Y. Qu, F. Ma, J. Zhou, Bioresour. Technol. 166 (2014) 79–86.
[2] W. Zhang, C. Wei, G. An, Environ. Sci.: Processes Impacts 17 (2015) 975–984.
[3] Y. Du, M. Zhou, L. Lei, J. Hazard. Mater. 136 (2006) 859–865.
[4] F. Wang, Y. Hu, C. Guo, W. Huang, C.-Z. Liu, Bioresour. Technol. 110 (2012) 120–124.
[5] M. Zhang, J.H. Tay, Y. Qian, X.S. Gu, J. Environ. Eng. 123 (1997) 876–883.
[6] P. Lai, H.-z. Zhao, C. Wang, J.-r. Ni, J. Hazard. Mater. 147 (2007) 232–239.
[7] M.E. Sillanpä&#x00E4, T.A. Kurniawan, W.-h. Lo, Chemosphere 83 (2011) 1443–1460.
[8] A. Aydin, M. Altinbas, M. Sevimli, I. Ozturk, H. Sarikaya, Water Sci. Technol. 46 (2002) 323–330.
[9] A. Mahiroglu, E. Tarlan-Yel, M.F. Sevimli, J. Hazard. Mater. 166 (2009) 782–787.
[10] J. Schneider, M. Matsuoka, M. Takeuchi, J. Zhang, Y. Horiuchi, M. Anpo, D.W. Bahnemann, Chem. Rev. 114 (2014) 9919–9986.
[11] C. Zhai, M. Zhu, Y. Lu, F. Ren, C. Wang, Y. Du, P. Yang, Phys. Chem. Chem. Phys. 16 (2014) 14800–14807.
[12] T. Ochiai, A. Fujishima, J. Photochem. Photobiol. C 13 (2012) 247–262.
[13] Y. Zhang, Q. Wang, J. Lu, Q. Wang, Y. Cong, Chemosphere 162 (2016) 55–63.
[14] C. Zhai, M. Zhu, F. Ren, Z. Yao, Y. Du, P. Yang, J. Hazard. Mater. 263 (2013) 291–298.
[15] H. Sun, G. Li, X. Nie, H. Shi, P.-K. Wong, H. Zhao, T. An, Environ. Sci. Technol. 48 (2014) 9412–9419.
[16] G. Li, X. Liu, H. Zhang, T. An, S. Zhang, A.R. Carroll, H. Zhao, J. Catal. 277 (2011) 88–94.
[17] X. Nie, G. Li, M. Gao, H. Sun, X. Liu, H. Zhao, P.-K. Wong, T. An, Appl. Catal. B 147 (2014) 562–570.
[18] N. Baram, D. Starosvetsky, J. Starosvetsky, M. Epshtein, R. Armon, Y. Ein-Eli, Electrochem. Commun. 9 (2007) 1684–1688.
[19] D. Zhou, Z. Chen, Q. Yang, X. Dong, J. Zhang, L. Qin, Sol. Energ. Mater. Sol. Cells 157 (2016) 399–405.
[20] I. Paramasivam, H. Jha, N. Liu, P. Schmuki, Small 8 (2012) 3073–3103.
[21] Y. Zhou, Q. Yi, M. Xing, L. Shang, T. Zhang, J. Zhang, Chem. Commun. 52 (2016) 1689–1692.
[22] P. Song, X. Zhang, M. Sun, X. Cui, Y. Lin, Nanoscale 4 (2012) 1800–1804.
[23] C. Dong, M. Xing, J. Zhang, J. Phys. Chem. Lett. 7 (2016) 2962–2966.
[24] Y. Tang, S. Luo, Y. Teng, C. Liu, X. Xu, X. Zhang, L. Chen, J. Hazard. Mater. 241 (2012) 323–330.
[25] D. Pan, C. Xi, Z. Li, L. Wang, Z. Chen, B. Lu, M. Wu, J. Mater. Chem. A 1 (2013) 3551–3555.
[26] X. Wang, K. Maeda, X. Chen, K. Takanabe, K. Domen, Y. Hou, X. Fu, M. Antonietti, J. Am. Chem. Soc. 131 (2009) 1680–1681.
[27] X. Wang, K. Maeda, A. Thomas, K. Takanabe, G. Xin, J.M. Carlsson, K. Domen, M. Antonietti, Nat. Mater. 8 (2009) 76–80.
[28] G. Liu, P. Niu, C. Sun, S.C. Smith, Z. Chen, G.Q. Lu, H.-M. Cheng, J. Am. Chem. Soc. 132 (2010) 11642–11648.
[29] E.Z. Lee, Y.S. Jun, W.H. Hong, A. Thomas, M.M. Jin, Angew. Chem. Int. Ed. 49 (2010) 9706–9710.
[30] W.-J. Ong, L.-L. Tan, Y.H. Ng, S.-T. Yong, S.-P. Chai, Chem. Rev. 116 (2016) 7159–7329.
[31] C. Pan, J. Xu, Y. Wang, D. Li, Y. Zhu, Adv. Funct. Mater. 22 (2012) 1518–1524.
[32] D. Chen, K. Wang, T. Ren, H. Ding, Y. Zhu, Dalton Trans. 43 (2014) 13105–13114.
[33] D. Lu, G. Zhang, Z. Wan, Appl. Surf. Sci. 358 (2015) 223–230.
[34] J. Xu, L. Zhang, R. Shi, Y. Zhu, J. Mater. Chem. A 1 (2013) 14766–14772.
[35] M. Zhang, J. Xu, R. Zong, Y. Zhu, Appl. Catal. B 147 (2014) 229–235.
[36] X. Zhao, Y. Zhu, Environ. Sci. Technol. 40 (2006) 3367–3372.
[37] Y. Wang, R. Shi, J. Lin, Y. Zhu, Environ. Sci. Technol. 4 (2011) 2922–2929.
[38] J. Li, Y. Liu, H. Li, C. Chen, J. Photochem. Photobiol. A: Chem. 317 (2016) 151–160.
[39] Y. Li, R. Jin, X. Fang, Y. Yang, M. Yang, X. Liu, Y. Xing, S. Song, J. Hazard. Mater. 313 (2016) 219–228.
[40] W. Zhang, X. Xiao, Y. Li, X. Zeng, L. Zheng, C. Wan, Appl. Surf. Sci. 389 (2016) 496–506.
[41] X. Bai, L. Wang, Y. Wang, W. Yao, Y. Zhu, Appl. Catal. B 152 (2014) 262–270.
[42] X.-F. Gao, W.-T. Sun, Z.-D. Hu, G. Ai, Y.-L. Zhang, S. Feng, F. Li, L.-M. Peng, J. Phys. Chem. C 113 (2009) 20481–20485.
[43] Y. Hou, Z. Wen, S. Cui, X. Guo, J. Chen, Adv. Mater. 25 (2013) 6291–6297.
[44] X. Wang, S. Jin, H. An, X. Wang, Z. Feng, C. Li, J. Phys. Chem. C 119 (2015) 22460–22464.
[45] B. Lu, Y. Zhu, Phys. Chem. Chem. Phys. 16 (2014) 16509–16514.
[46] Y. Sun, Z. Sun, S. Gao, H. Cheng, Q. Liu, F. Lei, S. Wei, Y. Xie, Adv. Energy Mater. 4 (2014) 1300611.
[47] X. Chen, Y.-S. Jun, K. Takanabe, K. Maeda, K. Domen, X. Fu, M. Antonietti, X. Wang, Chem. Mater. 21 (2009) 4093–4095.
[48] F. Liang, Y. Zhu, Appl. Catal. B 180 (2016) 324–329.
[49] X. Yu, R. Xu, C. Wei, H. Wu, J. Hazard. Mater. 302 (2016) 468–474.
[50] S. Cao, J. Low, J. Yu, M. Jaroniec, Adv. Mater. 27 (2015) 2150–2176.
[51] H. Lee, W. Choi, Environ. Sci. Technol. 36 (2002) 3872–3878.
[52] Z. Wei, Y. Liu, J. Wang, R. Zong, W. Yao, J. Wang, Y. Zhu, Nanoscale 7 (2015) 13943–13950.
[53] W. Liu, M. Wang, C. Xu, S. Chen, X. Fu, J. Mol. Catal. A: Chem. 368 (2013) 9–15.
[54] O. Simond, V. Schaller, C. Comninellis, Electrochim. Acta 42 (1997) 2009–2012.
[55] R. Pelegrini, J. Reyes, N. Duran, P. Zamora, A. De Andrade, J. Appl. Electrochem. 30 (2000) 953–958.